Supporting Information

Rh-doped Pt-Ni octahedral nanoparticles: understanding the correlation between elemental distribution, ORR and shape stability

Experimental part

Chemicals and materials

Platinum(II)acetylacetonate ($Pt(acac)_2$, Pt 48% min.), nickel(II)acetylacetonate ($Ni(acac)_2$, 95.0 %), tungsten hexacarbonyl ($W(CO)_6$, 97.0 %) and oleic acid (OAc, 90.0 %) were obtained from Alfa Aesar. Rhodium(III)acetylacetonate ($Rh(acac)_3$, 97.0 %), oleylamine (OAm, 70.0 %) and acetic acid (HAc, ≥ 99.9 %) were obtained from Sigma Aldrich. Dibenzylether (Bn_2O, 98.0 %) was obtained from Fluka, ethanol (100.0 %) from VWR Chemicals and toluene (99.8 %) from Roth. All chemicals were used as received.

Synthesis of Pt-Rh-Ni/C and Pt-Ni/C oct

To prepare *Pt-Rh-Ni* octahedral nanoparticles $Pt(acac)_2$ (0.102 mmol), $Ni(acac)_2$ (0.234 mmol), OAm (12 mL) and OAc (8 mL) were added into a 100 ml three-neck-flask under reflux. The reaction mixture was stirred for 5 minutes under nitrogen atmosphere at 60 °C, followed by raising the temperature to 130 °C. At this temperature $W(CO)_6$ (0.389 mmol) was added rapidly, nitrogen purging was stopped and the reaction mixture was heated to 230 °C and then stirred for 30 minutes. Afterwards $Rh(acac)_3$ (0.017 mmol) dissolved in Bn_2O (3 mL) was added and stirred for additional 20 minutes at 230 °C. Then the reaction mixture was cooled down to room temperature and toluene (10 mL) and ethanol (30 ml) were added to the reaction mixture. The supernatant was removed by centrifugation (7800 rpm for 5 min) and dispersed in toluene (20 mL). The dispersion was added to a dispersion of Vulcan XC 72R (0.04 g) in toluene (20 mL). The mixture was sonicated with an ultrasonic horn for 1 h. Afterwards ethanol (10 mL) was added and the Pt-Rh-Ni/C catalyst was centrifuged (7800 rpm for 10 min). The resulting particles were added into acetic acid (40 mL) and refluxed for 30 min at 60 °C. After the mixture was cooled down the particles were washed with ethanol (30 mL) three times and dried for 12 h on air.

To prepare *Pt-Ni/C* octahedral nanoparticles $Pt(acac)_2$ (0.078 mmol), $Ni(acac)_2$ (0.234 mmol), OAm (12 mL) and OAc (8 mL) were added into a 100 ml three-neck-flask under reflux. The reaction mixture was stirred for 5 minutes under nitrogen atmosphere at 60 °C, followed by raising the temperature to 130 °C. At this

temperature $W(CO)_6$ (0.389 mmol) was added rapidly, nitrogen purging was stopped and the reaction mixture was heated to 230 °C and then stirred for 40 minutes. The following procedure was the same like for the Pt-Rh-Ni octahedral nanoparticles.

Physico-chemical Characterization

XRD: X-ray diffraction patterns were collected on a Bruker D8 Advance (Siemens KFL Cu 2K X-ray tube and Lynx Eye Detektor) diffractometer in Bragg Brentano geometry using a Cu Kα1. The patterns were recorded between 20-80° with a step size of 0.05° and a 10 s measurement time at each step.

ICP OES: An inductively coupled plasma analysis system was used to determine the elemental composition of the synthesized particles. The selected wavelengths for the concentration determination were 203.646; 214.424; 224.552; 265.945; 306.471 nm for Pt, 216.555; 221.648; 222.295; 222.486; 227.021; 230.299; 231.604 nm for Ni and 233.477; 246.103; 249.078; 343.488; 369.236 nm for Rh.

Scanning transmission electron microscopy (STEM) was performed using a Cs-probe corrected FEI Titan 80-200 ("ChemiSTEM") and double Cs-corrected JEOL JEM-ARM200CF microscopes. The both microscopes were operated at 200 kV. In order to achieve "Z-Contrast" conditions, a probe semi-angle of 25 mrad and an inner collection semi-angle of the detector of 88 mrad were used. Compositional maps were obtained with energy-dispersive X-ray spectroscopy (EDX) using four large-solid-angle symmetrical Si drift detectors. For EDX elemental mapping, Pt L, Ni K and Rh L peaks were used. The error of the EDX composition measurement for individual particles after a typical investigation of 15 minutes is about +/- 2 at.%.

Catalyst ink preparation: To prepare an ink 4 mg of catalyst were added into 2.5 mL water, 15 µL Nafion (5 wt%) and 0.5 mL *iso*propanol (≥ 99.5 %) and ultrasonicated for 15 minutes. 10 µL of the ink were placed on a glassy carbon rotating disk electrode, which results in a Pt loading of 16 µg cm^{-2}. The film was dried at 50 °C for 7 minutes.

Electrochemical Characterization: For electrochemical characterizations a conventional three electrode cell with a Pt gauze as counter electrode (Pt furled Pt 5x5 cm^2 mesh), a reference electrode (MMS Hg/Hg_2SO_4 with the potential E= -0.722 V Vs. RHE) and a glassy carbon working electrode (5 mm diameter) was used. The working electrode always was lowered into the electrolyte under potential control at 0.05 V vs. RHE. A 0.1 M $HClO_4$ was used for electrochemical measurements (diluted from 70 % conc. $HClO_4$, 99.999 % trace metal bases, Sigma Aldrich with milli-Q water). All measurements were performed with a BioLogics Science

Instruments potentiostat SP-150 and SP-200. The degree of purity for the used gases was 99.998 % for oxygen, 99.999 % for nitrogen and 99.999 % for hydrogen.

Activation Step: The electrochemical activation was performed via potential cycling between 0.05 and 1.0 V vs. RHE with a scan rate of 100 mV s^{-1} for 20 times under nitrogen atmosphere.

H_{upd}-ECSA Evaluation: To evaluate the H_{upd} based ECSA the last cycle which was recorded with 100 mV s^{-1} before activity measurements was selected. The cyclic voltammetry was performed between 0.05 and 1.0 V vs. RHE with a scan rate of 100 mV s^{-1} under nitrogen atmosphere. The values were calculated integrating the cyclic voltammogram (CV) between 0.05 and 0.4 V. The measured Q_H value was normalized with respect to the theoretical value of Q_H^{theo} = 210 µC cm^{-2}, which is assuming a one electron transfer between one H atom and one Pt atom.

Catalytic Acitivity for Oxygen Reduction Reaction: The catalytic activity of the catalysts was measured by linear sweep voltammetry. It was performed in oxygen saturated electrolyte (at least 15 minutes bubbled) in a potential range between 0.05 and 1.0 V vs. RHE with a scan rate of 10 mV s^{-1} and a rotation speed of 1600 rpm. The kinetic currents were calculated using the equation,

$$\frac{1}{j} = \frac{1}{j_k} + \frac{1}{j_d}$$

where j was measured at 0.9 V and j_d was determined in the diffusion limited current area and j_k is the calculated kinetic current density. The presented results are iR corrected, where the resistance R was determined by potential electrochemical impedance spectroscopy at 0.4 V vs. RHE.

Stability Measurements: Stability measurements for 4k and 8k cycles have been performed via potential cycling between 0.5 and 1.0 V vs. RHE with a scan rate of 50 mV s^{-1} and stability measurements for 30k cycles have been performed between 0.6 and 1.0 V vs. RHE with 100 mV s^{-1} in deaerated electrolyte. Before and after each stability protocol, three CV between 0.05 and 1.0 V vs. RHE with 100 mV s^{-1} were performed.

CO-Oxidation: For CO oxidation the electrolyte was saturated with nitrogen for 15 minutes. Afterwards the working electrode was lowered into the electrolyte under potential control at 0.05 V vs. RHE and the electrolyte was bubbled with nitrogen for additional 5 minutes. Then the gas was switched to CO and the bubbling occurs for another 15 minutes followed by a gas change to nitrogen again in order to remove CO from the electrolyte. Two cyclic voltammograms were recorded between 0.06 and 1.0 V with 50 mV s^{-1} and 400 rpm.

Additional information

Table S1 Evaluation of XRD data as well as the calculated 2Θ values calculated from the ideal Vegard's law, using a bimetallic alloy of *Pt-Rh-Ni*.

$Pt_{81}Ni_{19}$/C oct			
hkl	**d**	**$2\Theta_{theo}$**	**$2\Theta_{real}$**
111	2.22	40.57	40.83
200	1.92	47.23	47.23
220	1.36	69.02	69.43
$Pt_{71}Rh_3Ni_{26}$/C oct ($Pt_{73}Ni_{27}$ assumption)			
hkl	**d**	**$2\Theta_{theo}$**	**$2\Theta_{real}$**
111	2.20	40.94	40.74
200	1.91	47.63	47.32
220	1.35	69.65	69.29

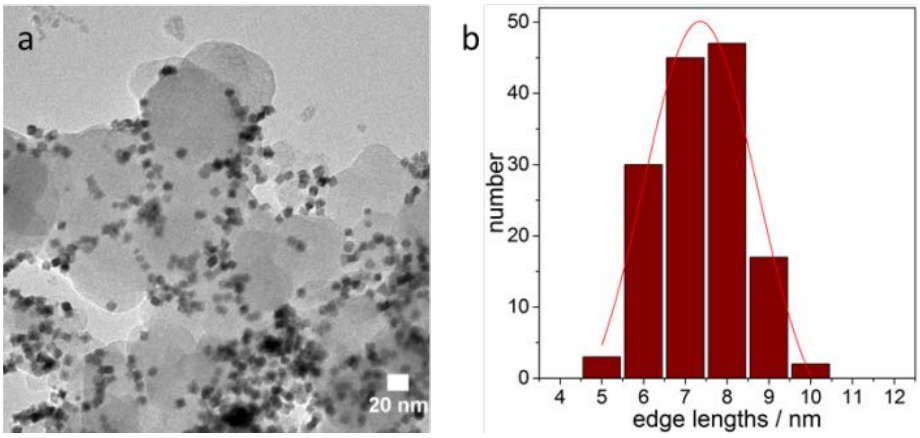

Figure S1 a) Overview of *Pt-Rh-Ni* octahedral nanoparticles distribution on carbon and b) particle size distribution of *Pt-Rh-Ni/C* particles (based on 144 particles) with average edge length of 7.4 ± 1.0 nm, obtained from the fitted profile (Gaussian distribution).

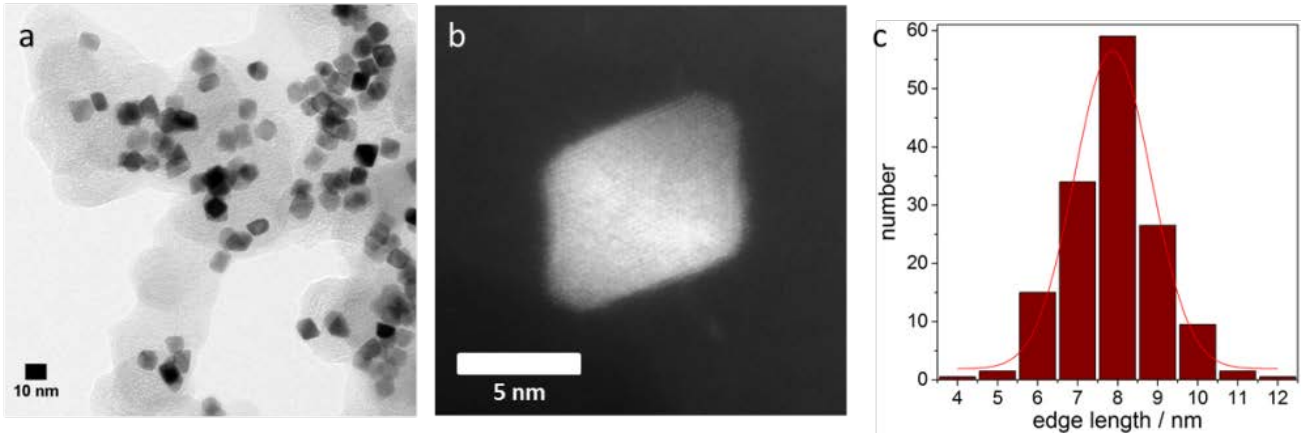

Figure S2 Transmission electron microscopy images of *Pt-Ni/C* after synthesis and acetic acid treatment. a) overview of the particles with a homogeneous distribution and mainly octahedral shaped nanoparticles, b) STEM image of *Pt-Ni/C*, c) Particle size distribution of *Pt-Ni/C* octahedral nanoparticles (based on 296 particles) with average edge length of 7.9 ± 1.1 nm, obtained from the fitted profile (Gaussian distribution).

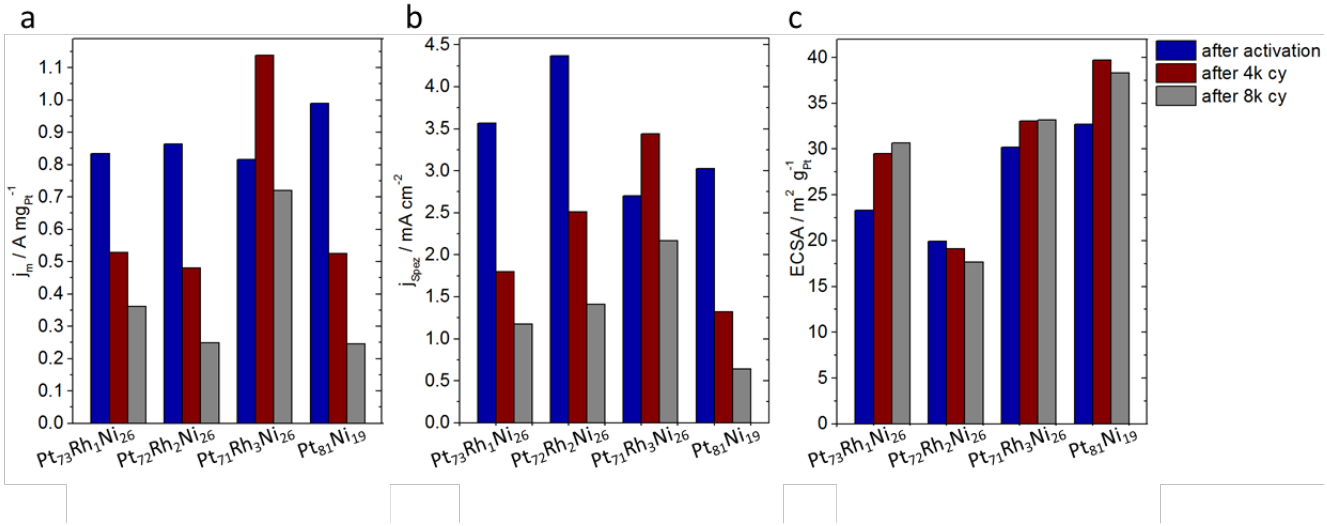

Figure S3 Electrochemical characterization and effect of the amount Rh on the: a) mass based activities, b) specific activities based on H_{upd}-ECSA and c) H_{upd} ECSA after 20 cycles (cy) activation, 4k and 8k cycles (cy) stability test (LSV: 0.05 – 1.0 V vs. RHE with 10 mV s^{-1} in O_2 saturated 0.1 M $HClO_4$ electrolyte, 1600 rpm, evaluated at 0.9 V; CV: 0.05 – 1.0 V vs. RHE with 100 mV s^{-1} in N_2 saturated 0.1 M $HClO_4$ electrolyte, 0 rpm).

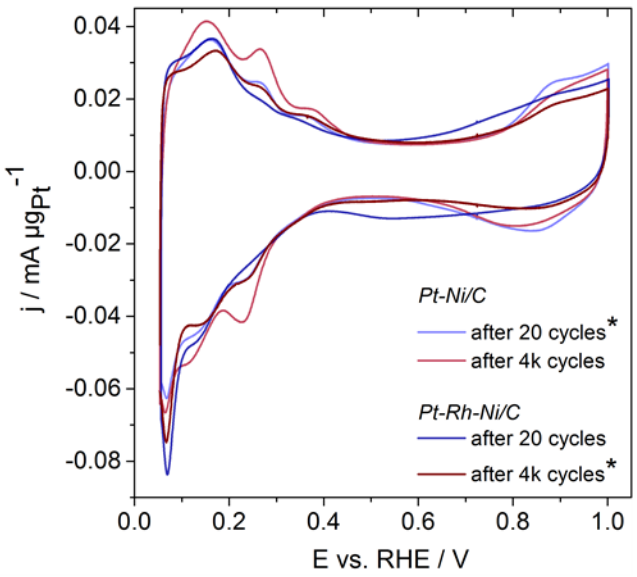

Figure S4 Comparison of CVs of the *Pt-Ni/C* and the *Pt-Rh-Ni/C* catalyst after activation and after 4k cycles stability, * is indicating the most active states, respectively, where shape of the CVs looks quite similar in the H_{upd} region.

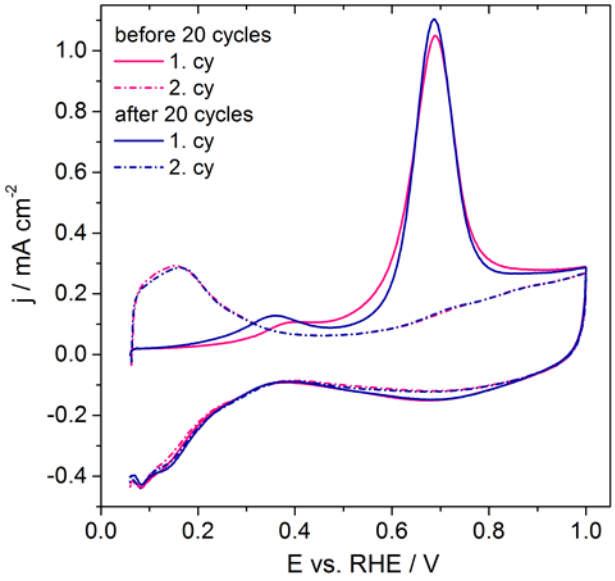

Figure S5 CO-Oxidation experiment of the *Pt-Rh-Ni/C* catalyst before and after 20 cycles activation; 0.05-1.0 V vs. RHE with 50 mV s^{-1} in N_2 saturated 0.1 M $HClO_4$.

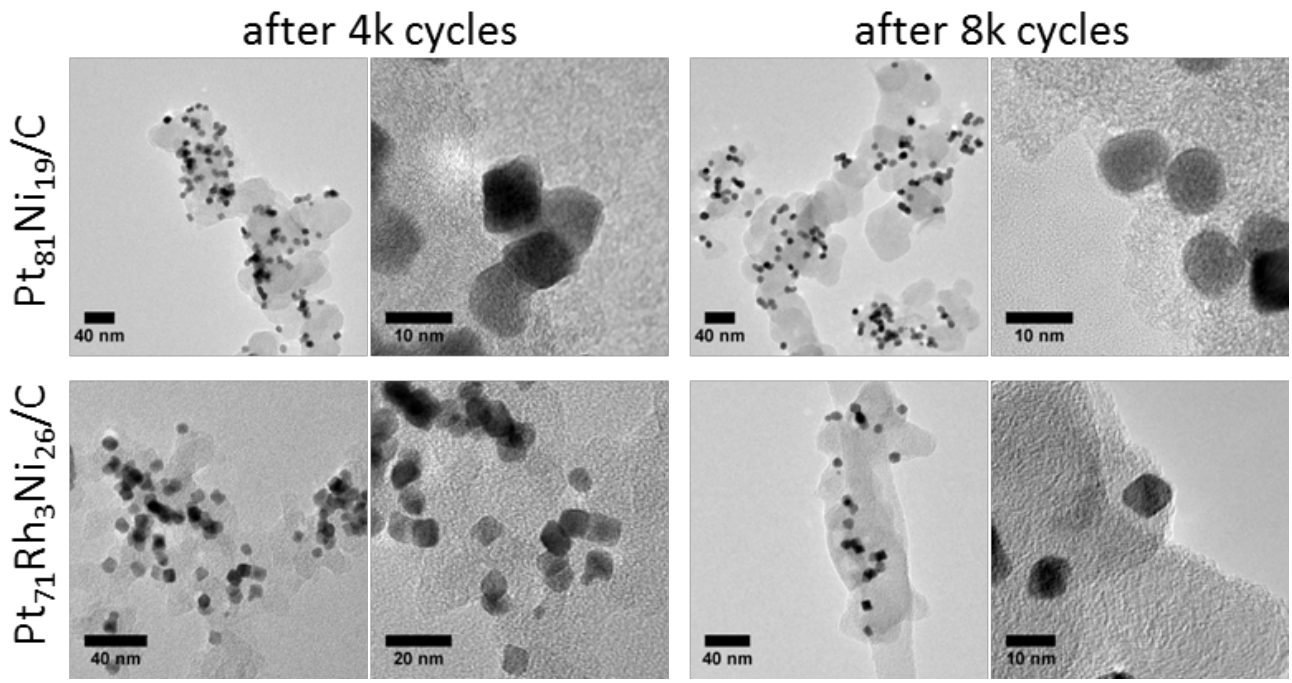

Figure S6 TEM images for the comparison of shape stability of the pure *Pt-Ni/C* catalyst and the *Pt-Rh-Ni/C* catalyst after 4k and after 8k cycles stability test.

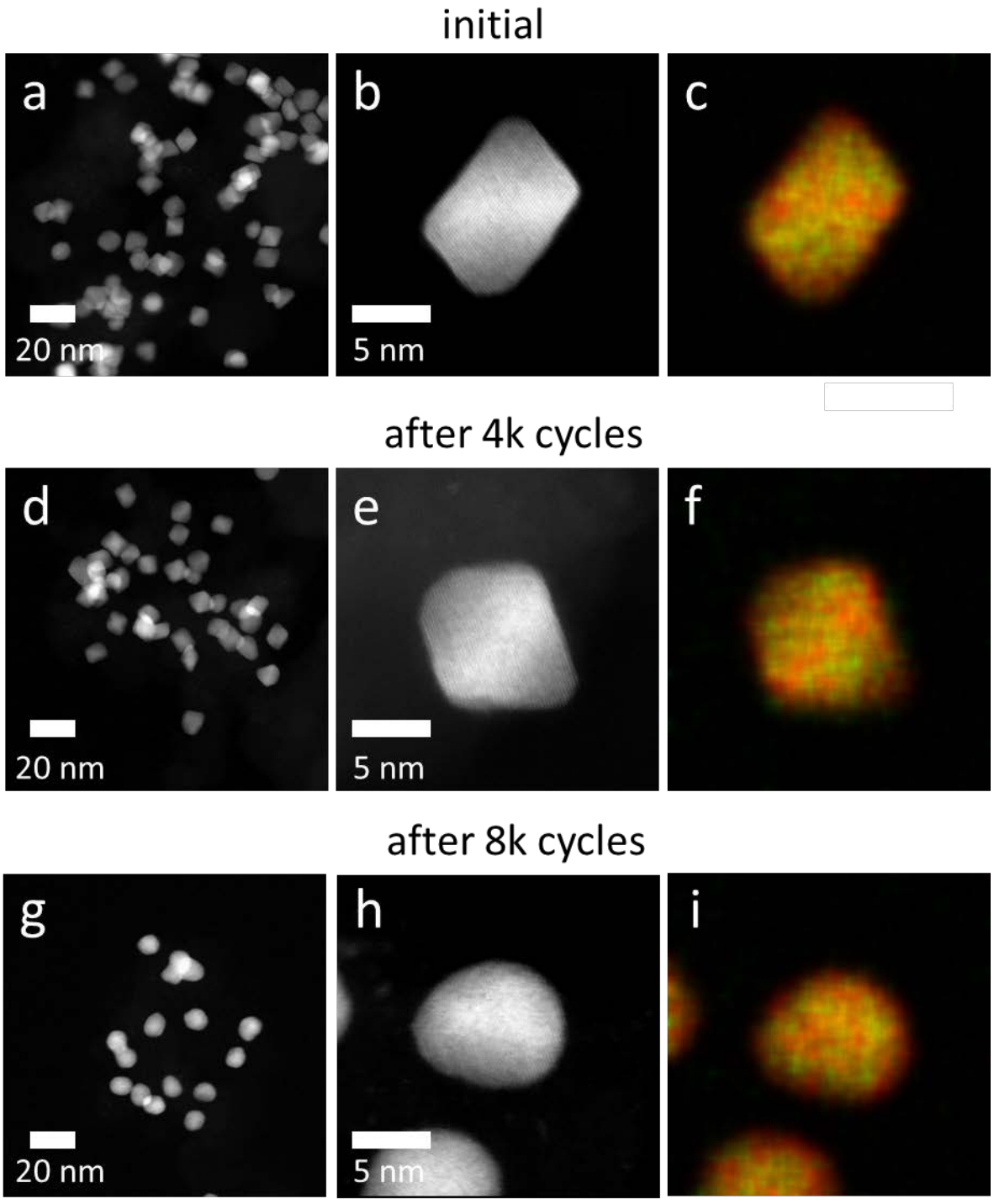

Figure S7 HAADF STEM images and EDX composition maps of *Pt-Ni* nanoparticles. a, d, g HAADF STEM overview images of the nanoparticles in the initial state (a), after 4 k cycles (d), and after 8 k cycles (g). b, e, h, High resolution HAADF STEM images of *Pt-Ni* octahedral nanoparticles in different states. c, f, i Pt (red) and Ni (green) EDX composition map of the corresponding nanoparticles.

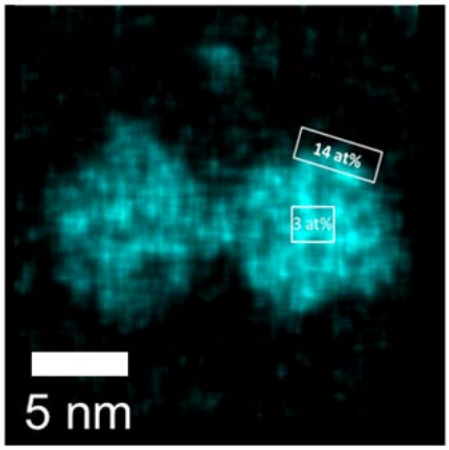

Figure S8 Rh distribution in an EDX composition map of initial *Pt-Rh-Ni* nanoparticles. The amount of Rh in atomic percent is indicated in the corresponding area (white boxes).

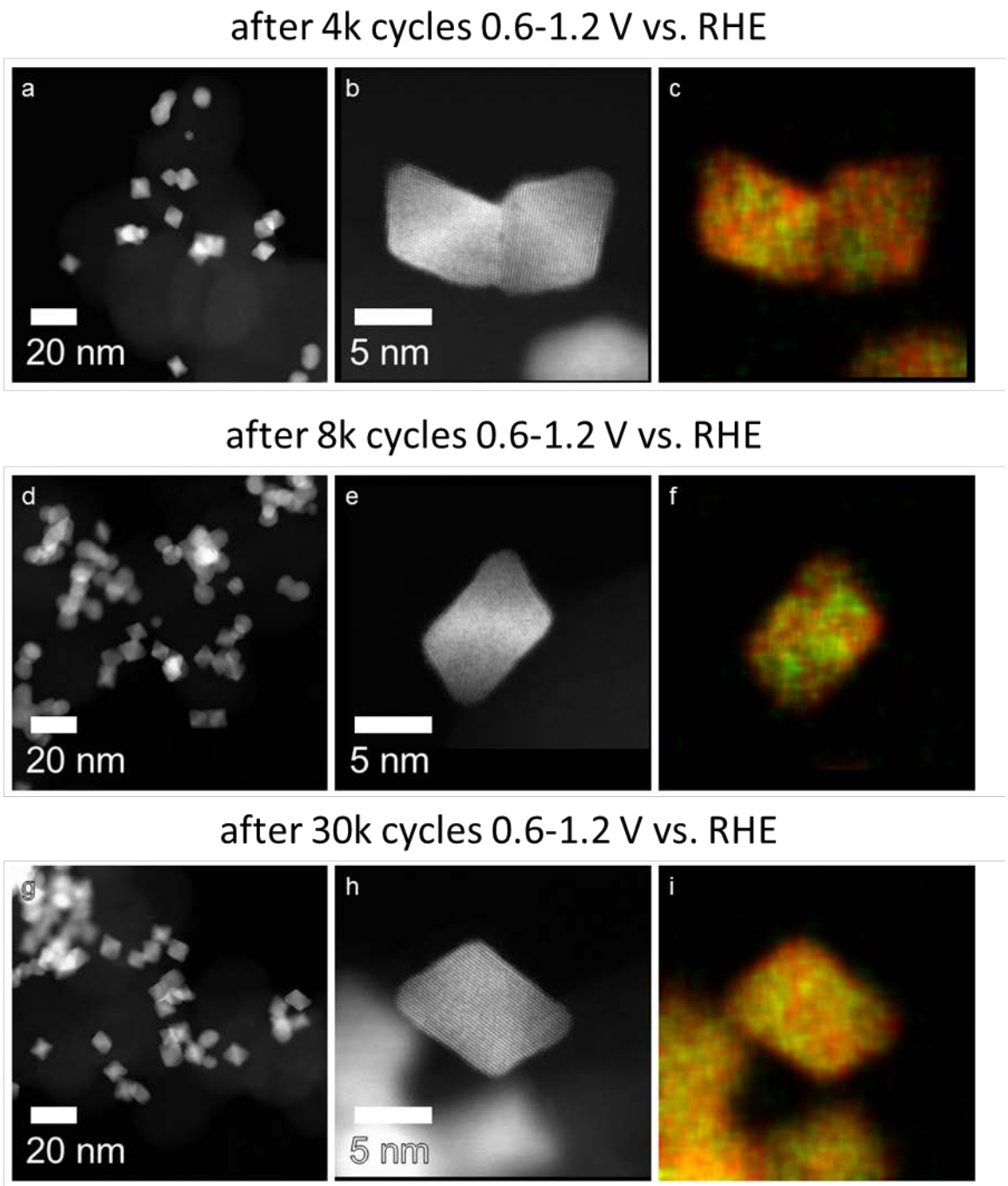

Figure S9 HAADF STEM images and EDX composition maps of *Pt-Rh-Ni* octahedral nanoparticles after 4 k cycles (a,b,c), after 8 k cycles (d,e,f) and after 30 k cycles (g,h,i) between 0.6 and 1.2 V vs. RHE. Overview HAADF STEM images (a,d,g) and high resolution HAADF STEM images of PtNiRh octahedral nanoparticles oriented close to ⟨110⟩ (b,e,h). Pt (red) and Ni (green) EDX composition maps of the corresponding octahedral nanoparticles (c,f,i).

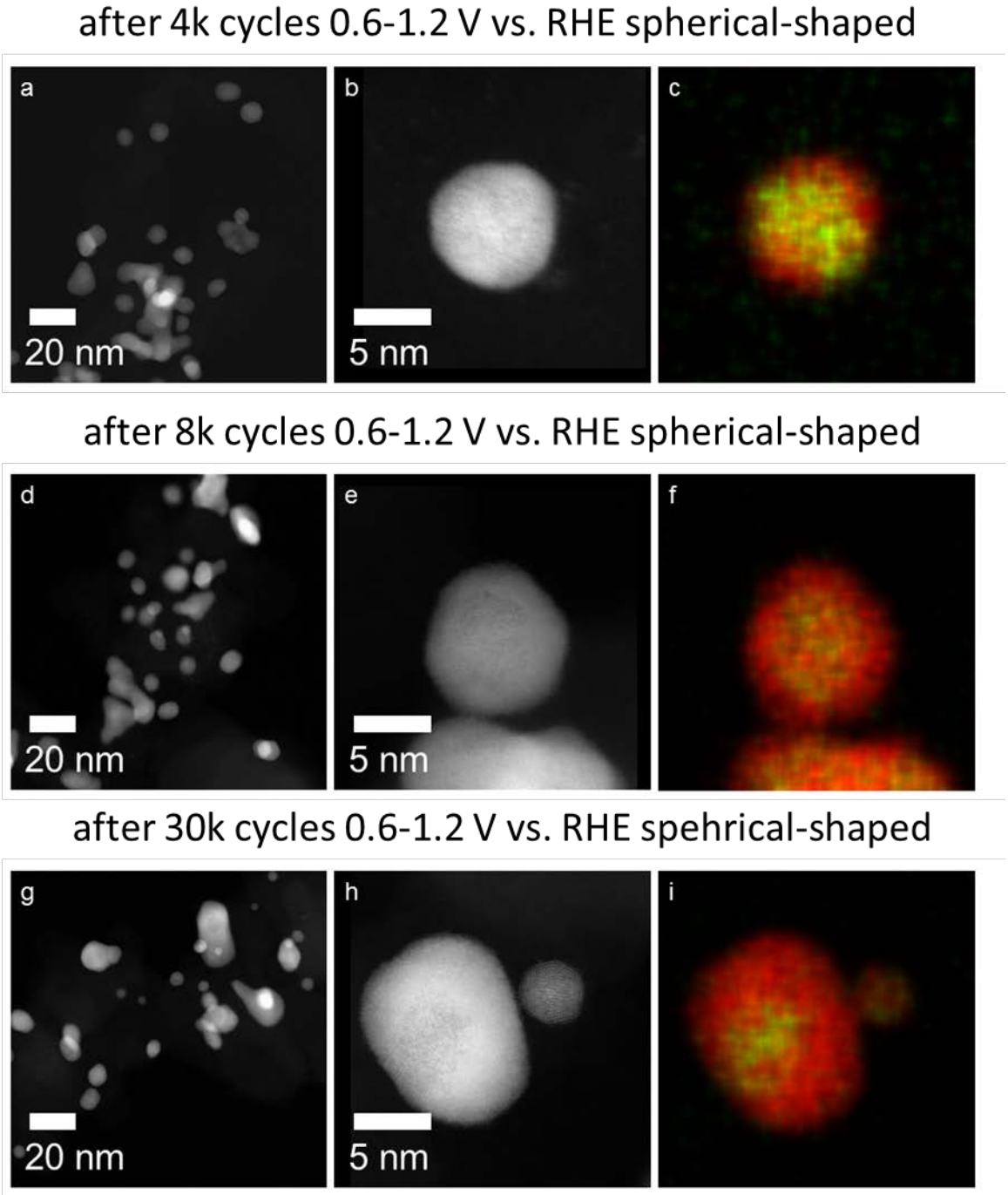

Figure S10 HAADF STEM images and EDX composition maps of spherical-shaped *Pt-Rh-Ni* nanoparticles after 4 k cycles (a,b,c), after 8 k cycles (d,e,f) and after 30 k cycles (g,h,i) between 0.6 and 1.2 V vs. RHE. Overview (a,d,g) and high resolution HAADF STEM images (b,e,h) as well as Pt (red) and Ni (green) EDX composition maps of the corresponding nanoparticles (c,f,i).

Figure S9 and Figure S10 show HAADF STEM images and EDX composition maps of the respective *Pt-Rh-Ni* nanoparticles. Figure S9 indicates that octahedral nanoparticles with a similar Pt and Ni distribution and composition are present as for the nanoparticles cycled between 0.05 and 1.0 V vs. RHE. With an increasing number of cycles, the segregated structure is lost and a more homogeneously alloyed nanoparticle structure is observed. However, after applying potential cycles between 0.6 and 1.2 V vs. RHE additional spherical-shaped particles are found with a Ni-rich core and a Pt-rich shell (Figure S10). The core-shell structure is clearly visible in the EDX maps (especially in Figure S10 f and i) as well as by the contrast difference in the HAADF STEM images (Figure S10 e and h). In the spherical-shaped nanoparticles most of the Ni is leached out due to the higher potential over 1.1 V and only a small Ni content between 7 and 16 at.% remains. In contrast to the application of cycles between 0.5 and 1.0 V vs. RHE, it is obvious that after the cycles between 0.6 and 1.2 V vs. RHE, a mixture of octahedral and spherical-shape particles is observed. Interestingly, only the octahedral nanoparticles retain a high Ni content.

Possible reasons for the formation of these heavy degraded particles could be (i) less Rh accumulation in the outer novel metal shell in the initial particle and therefore a change in the Pt diffusion rate behavior during electrochemical cycling or (ii) a slightly thinner Pt-Rh shell in the initial particles. Applying a potential higher than 1.0 V on these “defect” particles changes the diffusion rate behavior of Pt and therefore might inducing the dissolution of Ni. As soon as only small amounts of Ni are able to reach the surface and thereby to dissolve from the particle, pin-holes are built and a strong degradation process is taking place. In comparison, the particles which are still octahedral after stability measurements up to 1.2 V vs. RHE, seems to exhibit a Pt-Rh shell still thick enough to protect Ni from leaching. As a result, they are not undergoing a structural degradation process, and are showing a similar behavior, i.e. structural rearrangement of Pt and Ni atoms, losing of favorable Ni segregation directly beneath of Pt-Rh shell, like the particles only cycled up to 1.0 V.